Aerospace Science and Technology 111 (2021) 106549

Contents lists available at ScienceDirect

Aerospace Science and Technology

www.elsevier.com/locate/aescte

Distributed sliding mode control for time-varying formation tracking of multi-UAV system with a dynamic leader ☆

Jianhua Wang [a], Liang Han [a,*], Xiwang Dong [b], Qingdong Li [b], Zhang Ren [b]

[a] Sino-French Engineer School, Beihang University, Beijing, China
[b] School of Automation Science and Electronic Engineering, Beihang University, Beijing, China

ARTICLE INFO

Article history:
Received 20 August 2020
Received in revised form 31 December 2020
Accepted 25 January 2021
Available online 29 January 2021
Communicated by Xingqun Zhan

Keywords:
Distributed sliding mode control
Formation tracking control
Multi-agent system
Coordinated control
Unmanned aerial vehicle (UAV)

ABSTRACT

Time-varying formation tracking control problems for the multi-UAV system are investigated in this paper, where a leader with dynamic input is considered. Based on the sliding mode control theory, continuous-time and discrete-time distributed formation tracking protocols are proposed by utilizing the neighboring relative information. Using Lyapunov stability approach, sufficient conditions for the multi-UAV system to achieve the desired formation tracking are given and the width of quasi-sliding mode domain for the discrete-time protocol is expressed. Algorithms to construct the designed continuous-time and discrete-time protocols for multi-UAV systems are provided. Based on the Gazebo simulator, a formation tracking virtual experiment platform for multi-UAV systems is constructed. Virtual experiments with multiple UAVs are performed to demonstrate the effectiveness of the continuous and discrete formation tracking protocols.

1. Introduction

During the past few years, formation control technology of multi-agent systems has been extensively investigated and applied in broad domains, such as cooperative surveillance of aircrafts [1–3], attitude tracking of spacecrafts [4–7], collaborative load transport of robots [8–10]. With the development of various technologies, unmanned aerial vehicle (UAV), as a typical representative of agent, can accomplish more and more complicated missions [11–13]. To overcome the shortcomings of single UAV in mission, for instance, low efficiency, low performance, and high cost, the UAV swarm operations become a new trend, where multiple UAVs collaborate with each other and externally act as an entire system. As a representative of cooperative control technologies, formation control of multiple UAVs is an important research topic. For multi-UAV systems, how to realize the expected formation by a distributed and robust control method is of both theoretical challenges and engineering significances.

Due to the great advances in consensus control of multi-agent systems [14–17] over the past years, consensus based approach is extended to deal with the formation control problem of multi-UAV systems. In [18], the formation control problem of a team of Vertical Take-Off and Landing UAVs is investigated, where the communication delays among UAVs are considered. In [19], an output feedback linearization method is developed to deal with the time-varying formation control problem of multi-UAV systems. In [20], a consensus based approach is proposed for the time-varying formation control problem of multi-UAV systems, and the procedure to design the protocol is summarized. In [21], necessary and sufficient conditions for multi-UAV systems with topology switching to realize a time-varying formation are presented. It should be indicated that in [18–21], only formation control problems of multiple-UAV systems are taken into account.

In practical applications, only realizing the desired formation is not enough, but it is also required that the multi-UAV system can track the reference trajectory generated by a virtual or real leader. In this case, the formation tracking control problem for multi-UAV systems arises. In [22], a feedback formation control strategy is developed to deal with the formation tracking problem of UAVs. In [23], a two-layer control strategy is developed to deal with the time-varying formation tracking problem. In [24], a formation tracking control problem for

☆ This work was supported by the Science and Technology Innovation 2030-Key Project of "New Generation Artificial Intelligence" under Grant 2018AAA0102305, and the National Natural Science Foundation of China under Grants 61803014, 61922008, 61973013, and 61873011.

* Corresponding author.
E-mail address: liang_han@buaa.edu.cn (L. Han).

https://doi.org/10.1016/j.ast.2021.106549
1270-9638/

multi-UAV systems is investigated, where a collective control strategy is presented to guarantee the realization of trajectory tracking. In [25], a sliding mode controller is proposed for the formation tracking control problem of multi-UAV systems, and the performance of the controller is evaluated by conducting an experiment with a virtual leader and a real follower quadrotor UAV. In [26], the formation tracking control for multi-UAV systems is achieved by a learning-based model predictive controller that considers the unmodeled dynamics of the UAV. In [27], a protocol with time-varying delays using only neighboring relative position information is introduced to solve the formation tracking problem of multi-UAV systems. In [28], an optimal control approach is developed to deal with the formation trajectory tracking control problem of multi-UAV systems. In [29], time-varying formation tracking problem of multi-UAV systems with switching directed topology is studied, where a protocol that involves formation feasibility condition is provided to ensure the realization of the expected formation tracking. In [30], an adaptive control protocol is designed to solve the formation tracking problems of multi-UAV systems with parametric uncertainties and external disturbances. Based on back-stepping approach, a guidance control method is constructed in [31] to make multi-UAV systems realize the expected formation. In [32], a rolling optimization approach is proposed to deal with the formation tracking problem of multi-UAV systems, where the formation reconfiguration is taken into account. Note that the researches in [22–32] are based on continuous-time model and the proposed formation tracking protocol is of continuous form.

It should be pointed out that the continuous-time protocols cannot be employed directly because the digital system can only handle discretized signal. With the broad application of digital systems in engineering fields, the research on design of discrete-time protocol that can be implemented directly receives more and more attention. Thus, it is more interesting to investigate the formation tracking control problem with discrete-time model and to design the discretized protocol. In [33], a discrete-time formation control problem with switching topology is studied, where the link failures and actuator faults are taken into account. Necessary and sufficient conditions for multi-UAV systems to realize formation with one sample period delay are given in [34]. An adaptive backstepping approach that involves quantized signals for multi-UAV systems to achieve time-varying formation tracking is presented in [35]. In [36], discrete-time formation tracking control problems that consider the system nonlinearity is investigated. In [37], a consensus based state fusion estimation approach is developed to deal with the discrete-time formation problem of multi-UAV systems. In [38], an event-triggered method is proposed to handle the discrete-time formation tracking problems of multi-UAV systems, and the designed algorithm can remove the communication assumption. However, the common assumption in the above formation tracking control problem for multi-UAV systems is that the leader is without any control input [27–30,36], or the control input of the leader is known to the followers [23–25].

According to whether the leader's control input is known or not, the leader can be divided into cooperative and non-cooperative target. More specifically, when the control input of the leader can be obtained by the followers, the leader is called a cooperative target; when the leader's control input is unknown to the followers, the leader is called a non-cooperative target. The multi-UAV system formation tracking control technologies for non-cooperative targets have more extensive applications, for instance, the scenario where the police need to track and intercept an illegal UAV. Compared with the problems with cooperative targets, the formation tracking control problems of multiple-UAVs with non-cooperative targets are more complicated. In order to expand the potential applications of the multi-UAV formation tracking control technologies, the non-cooperative target, namely, the leader with unknown control input, is considered in this paper.

The time-varying formation tracking control problem for multi-UAV systems is investigated in this paper, where both continuous-time and discrete-time cases are studied. Based on the neighboring state information, sliding surface for each UAV in the multi-UAV system is designed. Using a sliding mode control approach, continuous-time and discrete-time formation tracking control protocols are proposed, respectively. Sufficient conditions for the multi-UAV system to realize the time-varying formation tracking are given. In addition, the quasi-sliding mode band for the discrete-time case is obtained. By using seven quadrotor UAVs in Gazebo simulator, virtual experiments with different sample time are conducted to verify the effectiveness of the proposed formation tracking method.

Compared with the previous researches, the main contributions of this paper are threefold. First, for the formation tracking control problem of multi-UAV systems, a leader with maneuvering acceleration is considered. Only the upper and lower bounds of the maneuvering acceleration need to be known. While in [23–30,36], it is assumed that the leader is without any control input or the control input of the leader is assumed to be known to the followers. Second, the UAV model and formation tracking protocol are constructed in continuous-time and discrete-time cases, respectively. Then, the discretized theoretical results can be directly applied to engineering fields. The researches in [24–26,28,29] are based on only continuous-time model, and the proposed protocol cannot be directly implemented in digital systems. Third, a virtual experiment formation tracking platform is constructed and the validity of the proposed protocols is demonstrated by virtual multi-UAV experiments. However, in [26–28,30,33–35], the effectiveness of protocols is verified by traditional numerical simulations. In contrast with the traditional simulations, the virtual experiments are closer to the actual application scenarios, and therefore the virtual experimental results are more meaningful for reference.

The rest of this paper is organized as follows. Preliminaries of graph theory and multi-UAV system modeling are introduced in section 2. The time-varying formation tracking problem description and transformation are described in section 3. Continuous and discrete formation tracking control protocols are proposed in section 4 and 5, respectively. In section 6, formation tracking virtual experiments with seven UAVs in Gazebo are performed. Conclusions are drawn in section 7.

Notations: sgn represents the symbolic function; $\mathrm{sgn}(A) = [\mathrm{sgn}(a_1), \mathrm{sgn}(a_2), \ldots, \mathrm{sgn}(a_n)]^{\mathrm{T}}$, if $A = [a_1, a_2, \ldots, a_n] \in \mathbb{R}^n$. In addition, $\|A\|$ denotes the Euclidean norm for a real vector A. $\mathbf{1}_n$ denotes an n-dimensional column vector with all elements being 1. $\otimes$ indicates the Kronecker product.

2. Preliminaries and system modeling

2.1. Graph theory

Consider a multi-UAV system with one leader labeled 0 and N followers labeled $1, 2, \ldots, N$. The interaction topology among the N followers can be described by a weighted directed graph $\mathcal{G} = (\mathcal{W}, \mathcal{E}, \mathcal{A})$, where $\mathcal{W} = \{w_1, w_2, \ldots, w_N\}$ denotes the set of nodes, $\mathcal{E} = \{e_{ij} = (w_j, w_i), w_i, w_j \in \mathcal{W}\}$ represents the set of edges, and $\mathcal{A} = [a_{ij}]_{N\times N}$ is the weighted adjacency matrix with $i, j \in \{1, 2, \ldots, N\}$. In addition, e_{ij} denotes the edge formed by nodes w_j and w_i, where w_j and w_i are called the parent node and child node, respectively. Moreover, $a_{ij} > 0$ represents the weight of edge e_{ij} if there exists $e_{ij} \in \mathcal{E}$, and $a_{ij} = 0$ if not. Besides, one assumes that $a_{ii} = 0, \forall i = 1, 2, \ldots, N$.

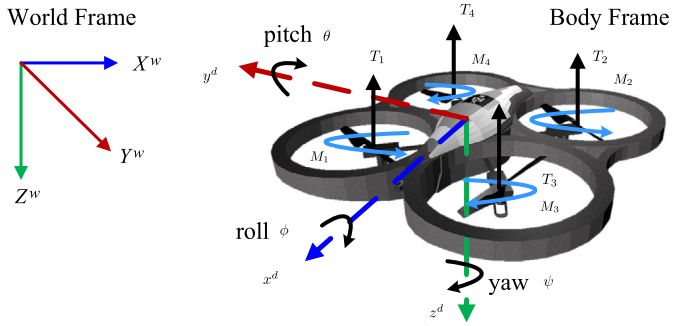

Fig. 1. Quadrotor UAV body diagram. (For interpretation of the colors in the figures, the reader is referred to the web version of this article.)

A *directed path* between nodes w_i and w_j is defined by a series of edges $(w_i, w_{i1}), (w_{i1}, w_{i2}), \ldots, (w_{il}, w_j)$, where $w_{ik}(k = 1, 2, \ldots, l)$ are different nodes of the graph. A directed graph $\mathcal{G}$ is said to have a *directed spanning tree* if there exists at least one node which has directed paths to all the other nodes. The in-degree of node w_i is defined as $\deg_{\text{in}}(w_i) = \sum_{j=1, j\neq i}^{N} a_{ij}$. Then the in-degree matrix $\mathcal{D}$ and the Laplacian matrix L are defined as $\mathcal{D} = \text{diag}(\deg_{\text{in}}(w_i), i = 1, 2, \ldots, N)$ and $L = \mathcal{D} - \mathcal{A}$, respectively.

Assume that the communication between the leader and followers is unidirectional, which means that the followers can get the status of the leader, but not vice versa. The interaction weight between the leader and follower i is denoted by a_{i0}. $a_{i0} > 0$ if the follower i can get the status of the leader, and $a_{i0} = 0$ if not. In addition, denote $H = \text{diag}(a_{10}, a_{20}, \ldots, a_{N0})$ and $L_H = L + H$.

Lemma 1. *If the directed graph $\mathcal{G}$ contains a directed spanning tree from the leader, then the matrix L_H is invertible.*

2.2. Quadrotor UAV modeling

For a quadrotor UAV, define the control input as

$$\begin{bmatrix} u_{c1} \\ u_{c2} \\ u_{c3} \\ u_{c4} \end{bmatrix} = \begin{bmatrix} T_1 + T_2 + T_3 + T_4 \\ T_2 - T_4 \\ T_1 - T_3 \\ M_1 - M_2 + M_3 - M_4 \end{bmatrix}, \tag{1}$$

where u_{c1}, u_{c2}, u_{c3}, and u_{c4} represent the total thrust perpendicular to the direction of the UAV body, the lift affecting the pitch and roll motion, and the torque affecting the yaw motion of the aircraft, respectively. M_i and T_i, $i = 1, 2, 3, 4$, are the torques and lifts generated by four different motors as marked in Fig. 1.

Next, we will derive the control model of the quadrotor UAV from two parts: translational motion and rotational motion [39,40].

2.2.1. Translational motion

According to Newton's second law, the dynamic equation of the UAV's translational motion can be described as

$$m \begin{bmatrix} \ddot{X}^w \\ \ddot{Y}^w \\ \ddot{Z}^w \end{bmatrix} = \begin{bmatrix} 0 \\ 0 \\ mg \end{bmatrix} + R_{b2w} \begin{bmatrix} 0 \\ 0 \\ -u_{c1} \end{bmatrix}, \tag{2}$$

where g is the acceleration of gravity and m denotes the mass of the UAV. X^w, Y^w, and Z^w are the North, East, and Down positions of UAV in the world frame, respectively. $R_{b2w} \in \mathbb{R}^{3\times3}$ is the transition matrix from the body frame to the world frame

$$R_{b2w} = \begin{bmatrix} \text{c}(\theta)\text{c}(\psi) & \text{c}(\psi)\text{s}(\phi)\text{s}(\theta) - \text{c}(\phi)\text{s}(\psi) & \text{s}(\phi)\text{s}(\psi) + \text{c}(\phi)\text{c}(\psi)\text{s}(\theta) \\ \text{c}(\theta)\text{s}(\psi) & \text{c}(\phi)\text{c}(\psi) + \text{s}(\phi)\text{s}(\theta)\text{s}(\psi) & \text{c}(\phi)\text{s}(\theta)\text{s}(\psi) - \text{c}(\psi)\text{s}(\phi) \\ -\text{s}(\theta) & \text{c}(\theta)\text{s}(\phi) & \text{c}(\phi)\text{c}(\theta) \end{bmatrix}, \tag{3}$$

where $\text{c}(\cdot)$ and $\text{s}(\cdot)$ represent $\cos(\cdot)$ and $\sin(\cdot)$; ϕ, θ, and ψ are the roll, pitch, and yaw angles, respectively.

Substituting R_{b2w} into (2), one has

$$\begin{cases} m\ddot{X}^w = u_{c1}(-\sin\phi\sin\psi - \cos\phi\sin\theta\cos\psi) \\ m\ddot{Y}^w = u_{c1}(\sin\phi\cos\psi - \cos\phi\sin\theta\sin\psi) \\ m\ddot{Z}^w = mg - u_{c1}\cos\phi\cos\theta \end{cases}. \tag{4}$$

2.2.2. Rotational motion

According to Euler's equations, the dynamic equation of the UAV's rotational motion can be described as

$$\tau = I^b\dot{\Omega} + \Omega \times I^b\Omega, \tag{5}$$

where τ denotes the total moment of the UAV, I^b represents the inertial tensor matrix, and $\Omega = [p, q, r]^{\text{T}}$ is the three-axis angular velocity of the UAV in the body frame. Due to the symmetrical layout characteristics of the quadrotor UAV, the inertial tensor matrix I^b can be

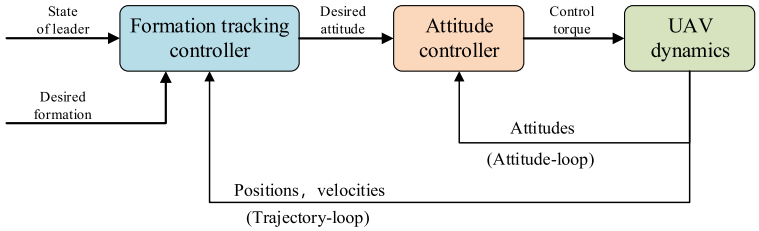

Fig. 2. Two loops control scheme for quadrotor UAV.

approximated as a diagonal matrix. Denote $I^b = \text{diag}\{I_{xx}, I_{yy}, I_{zz}\}$, where I_{xx}, I_{yy}, and I_{zz} are the components corresponding to the x, y, and z axes, respectively.

Consider the fact that

$$\tau = \begin{bmatrix} (T_2 - T_4)l \\ (T_1 - T_3)l \\ M_1 - M_2 + M_3 - M_4 \end{bmatrix} = \begin{bmatrix} u_{c2}l \\ u_{c3}l \\ u_{c4} \end{bmatrix}, \tag{6}$$

where l represents the distance from any motor to the body mass center. Since the symmetrical layout of the quadrotor UAV, l is also the half distance between the diagonal motors.

Denote $\Phi = [\phi, \theta, \psi]^{\mathrm{T}}$ as the attitude angle of UAV. The transformation relationship between the attitude angular velocity and three-axis angular velocity is

$$\dot{\Phi} = \begin{bmatrix} 1 & \sin\phi\tan\theta & \cos\phi\tan\theta \\ 0 & \cos\phi & -\sin\phi \\ 0 & \sin\phi/\cos\theta & \cos\phi/\cos\theta \end{bmatrix} \Omega. \tag{7}$$

When the roll and pitch angle are small enough, one has that $\dot{\Phi} \approx \Omega$, then (5) can be rewritten as

$$\begin{cases} I_{xx}\ddot{\phi} = u_{c2}l + \dot{\theta}\dot{\psi}(I_{yy} - I_{zz}) \\ I_{yy}\ddot{\theta} = u_{c3}l + \dot{\phi}\dot{\psi}(I_{zz} - I_{xx}) \\ I_{zz}\ddot{\psi} = u_{c4} + \dot{\phi}\dot{\theta}(I_{xx} - I_{yy}) \end{cases}. \tag{8}$$

Thus, it yields the complete four-input-six-output model of a quadrotor UAV (4) and (8). In general applications, assuming UAV flight near the hover state, it means that $\phi \approx 0$, $\theta \approx 0$, $\dot{\phi} \approx 0$, $\dot{\theta} \approx 0$, and $u_{c1} \approx mg$, a linearized model near the hover can be obtained

$$\begin{cases} \ddot{X}^w = (-\phi\sin\psi - \theta\cos\phi)g \\ \ddot{Y}^w = (-\theta\sin\psi + \phi\cos\phi)g \\ \ddot{Z}^w = -\frac{mg - u_{c1}}{m} \\ \ddot{\phi} = \frac{u_{c2}l}{I_{xx}} \\ \ddot{\theta} = \frac{u_{c3}l}{I_{yy}} \\ \ddot{\psi} = \frac{u_{c4}}{I_{zz}} \end{cases}. \tag{9}$$

In the linearized model (9), the coupling relationship between the four input and six output variables is decoupled. The control of the UAV's altitude and three-axis attitude is completely decoupled, and each channel is modeled as a second-order integrator. The horizontal position of the UAV is a second-order integrator of the roll angle and pitch angle after a linear transformation. In flight control and formation control of the quadrotor UAV, the system can be layered with independent control of each channel.

The control of the quadrotor UAV can be decoupled into attitude-loop control and trajectory-loop control. The corresponding controllers are called attitude and trajectory controllers, respectively. Fig. 2 shows the two loops control scheme for the quadrotor UAV. A PD controller will be used in the attitude-loop, and a formation tracking controller will be used in the trajectory-loop. Next, we will focus on the formation tracking control modeling for multiple UAVs.

2.3. Multi-UAV system modeling

In the trajectory-loop control, each UAV of the multi-UAV system can be simplified as

$$\begin{aligned} \dot{p}_i(t) &= v_i(t), \\ \dot{v}_i(t) &= u_i(t), \end{aligned} \tag{10}$$

where $i = 0, 1, 2, \ldots, N$, $p_i(t) \in \mathbb{R}^n$, $v_i(t) \in \mathbb{R}^n$, and $u_i(t) \in \mathbb{R}^n$ are the position, velocity, and control input of UAV i at time t, respectively.

For the sake of simplicity, let $n = 1$ in the following. However, it should be pointed out that all the theoretical analysis hereafter remains valid for higher dimensional cases, namely, $n \geq 2$.

Denote $x_i(t) = [p_i(t), v_i(t)]^{\mathrm{T}} \in \mathbb{R}^2$, the UAV i $(i = 0, 1, 2, \ldots, N)$ can be transformed to the following state space representation

$$\dot{x}_i(t) = Ax_i(t) + Bu_i(t), \tag{11}$$

where

$$A = \begin{bmatrix} 0 & 1 \\ 0 & 0 \end{bmatrix}, \ B = \begin{bmatrix} 0 \\ 1 \end{bmatrix}.$$

Let $X(t) = [x_1(t)^{\mathrm{T}}, x_2(t)^{\mathrm{T}}, \ldots, x_N(t)^{\mathrm{T}}]^{\mathrm{T}}$ and $U(t) = [u_1(t), u_2(t), \ldots, u_N(t)]^{\mathrm{T}}$, then the multi-UAV system with N followers can be written as

$$\dot{X}(t) = (I_N \otimes A)X(t) + (I_N \otimes B)U(t), \tag{12}$$

where I_N is identity matrix of size N.

The leader in the multi-UAV system has the same dynamics as the N followers. The control input $u_0(t)$ of the leader is dynamically changing but unknown to the followers.

Assumption 1. The dynamic input $u_0(t)$ of the leader is bounded, and there exist two constants $u_{\min}$ and $u_{\max}$ such that for all $t \geq 0$, $u_{\min} \leq u_0(t) \leq u_{\max}$.

Remark 1. The position and velocity of UAVs can be obtained accurately by sensors such as IRs and radars. However, the acceleration measure of UAVs contains various noises, thus is with low accuracy. The unknown acceleration of UAVs can be regarded as an unknown control input. Thus, we assume that the leader's positions and velocities are accessible to the followers while the leader's control input is unknown to the followers. Therefore, the theoretical results can be applied on the formation tracking control problems for non-cooperative targets.

Assumption 2. For the multi-UAV system (12), there exists at least one directed spanning tree from the leader.

Lemma 2. *[41] Consider a nonlinear system $\dot{y} = g(y)$, $g(0) = 0$, and a positive definite function $V(y) \in \mathbb{R}$. If there exist two constants α and γ such that*

$$\dot{V}(y) + \alpha V^{\gamma}(y) \leq 0, \tag{13}$$

with $\alpha > 0$ and $0 < \gamma < 1$, then $V(y)$ can reach zero in a finite period, where the finite setting time T depending on the initial state is

$$T \leq \frac{V^{(1-\gamma)}(y(0))}{\alpha(1-\gamma)}. \tag{14}$$

3. Problem statement and transformation

Definition 1. A time-varying formation for UAV i is specified by a vector $f_i(t) = [f_{ip}(t), f_{iv}(t)]^{\mathrm{T}} \in \mathbb{R}^{2\times 1}$, where $f_i(t)$ is continuously differentiable. $f_{ip}(t)$ and $f_{iv}(t)$ are the formation position and velocity components, respectively, and $\dot{f}_{ip}(t) = f_{iv}(t)$. The multi-UAV system (11) with one leader and N followers is said to achieve the formation tracking, if for any initial conditions and for all $i = 1, 2, \ldots, N$, there exists a constant $\sigma_f \geq 0$ such that

$$\lim_{t\to\infty} \|x_i(t) - f_i(t) - x_0(t)\| \leq \sigma_f, \tag{15}$$

where σ_f represents the formation tracking error boundary.

In order to describe the time-varying formation tracking scenario, let us consider an example with one leader and four followers. The expected formation among the followers is a square rotating counterclockwise. As shown in Fig. 3, the four followers form a square and the leader is located in the center of the square at time t_0, which means that the desired formation tracking is achieved. During the movement of the leader in the period from t_0 to t_1, the desired square formation among the four followers is maintained. At the same time, four followers track the trajectory of the leader and surround the leader in the center of the square. Since the square formation is turning counterclockwise, the relative position of the follower i with respect to the leader is changing according to the formation vector $f_i(t)$. It means that the expected time-varying formation tracking is realized.

Remark 2. The desired time-varying formation tracking consists of two aspects: on the one hand, the desired time-varying formation should be realized among the followers; on the other hand, the followers should be able to track the trajectory of the leader's movement. In fact, the leader can either be a real UAV to be tracked, or a virtual UAV used for generating a trajectory. For example, in Fig. 3, the leader indicated by the red hexagon is a real UAV. It should be pointed out that the formation vector $f_i(t)$ is not a global coordinate for the state $x_i(t)$ of follower i, but a relative offset with respect to the state $x_0(t)$ of the leader. The relationship between $f_i(t)$, $x_i(t)$, and $x_0(t)$ can be illustrated by the triangular formed by these three vectors in Fig. 3.

Define the following formation error system for UAV i,

$$\epsilon_i(t) = \sum_{j=1}^{N} a_{ij}(x_i(t) - f_i(t) - x_j(t) + f_j(t)) + a_{i0}(x_i(t) - f_i(t) - x_0(t)). \tag{16}$$

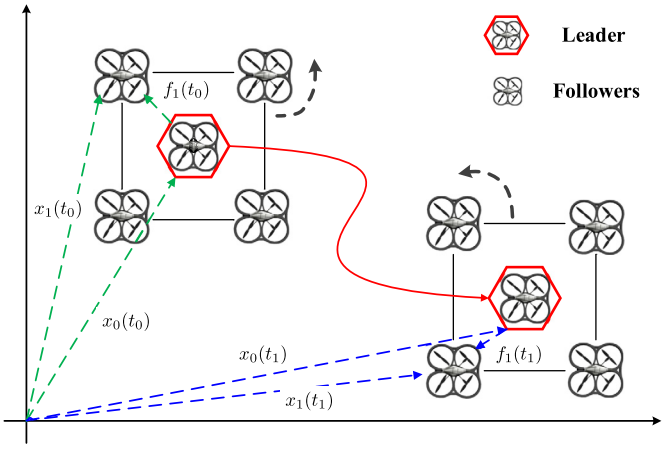

Fig. 3. Illustration of the time-varying formation tracking.

For sliding mode control approach, the switching function $s_i(t)$ for follower i is defined as

$$s_i(t) = K\epsilon_i(t), \tag{17}$$

where $K = [k_1, k_2] \in \mathbb{R}^{1\times 2}$ is the parameter matrix with $k_1 > 0$ and $k_2 > 0$.

Then the global switching function $S(t) = [s_1(t), s_2(t), \ldots, s_N(t)]^{\mathrm{T}}$ can be expressed as

$$S(t) = (L_H \otimes K)(X(t) - F(t)) - (H \otimes K)(\mathbf{1}_N \otimes x_0(t)), \tag{18}$$

with $F(t) = [f_1(t)^{\mathrm{T}}, f_2(t)^{\mathrm{T}}, \ldots, f_N(t)^{\mathrm{T}}]^{\mathrm{T}}$.

Lemma 3. *If the global switching function $S(t)$ reaches and remains on the sliding surface $S(t) = \mathbf{0}$, then the multi-UAV system (12) realizes the desired time-varying formation tracking defined by formation vector $F(t)$ and the formation tracking error boundary is $\sigma_f = 0$.*

Proof. According to error system (16), redefine the position and velocity formation error system for UAV i

$$\epsilon_{ip}(t) = \sum_{j=1}^{N} a_{ij}(p_i(t) - f_{ip}(t) - p_j(t) + f_{jp}(t)) + a_{i0}(p_i(t) - f_{ip}(t) - p_0(t)), \tag{19}$$

$$\epsilon_{iv}(t) = \sum_{j=1}^{N} a_{ij}(v_i(t) - f_{iv}(t) - v_j(t) + f_{jv}(t)) + a_{i0}(v_i(t) - f_{iv}(t) - v_0(t)). \tag{20}$$

Then one has $\epsilon_i(t) = [\epsilon_{ip}(t), \epsilon_{iv}(t)]^{\mathrm{T}}$ and $\dot{\epsilon}_{ip}(t) = \epsilon_{iv}(t)$. The switching function $s_i(t)$ in (17) can be rewritten as

$$s_i(t) = k_1\epsilon_{ip}(t) + k_2\epsilon_{iv}(t). \tag{21}$$

Denote $P(t) = [p_1(t), p_2(t), \ldots, p_N(t)]^{\mathrm{T}}$, $V(t) = [v_1(t), v_2(t), \ldots, v_N(t)]^{\mathrm{T}}$, $F_p(t) = [f_{1p}(t), f_{2p}(t), \ldots, f_{Np}(t)]^{\mathrm{T}}$, and $F_v(t) = [f_{1v}(t), f_{2v}(t), \ldots, f_{Nv}(t)]^{\mathrm{T}}$. In addition, let

$$\tilde{P}(t) = P(t) - F_p(t) - \mathbf{1}_N \otimes p_0(t), \tag{22}$$

$$\tilde{V}(t) = V(t) - F_v(t) - \mathbf{1}_N \otimes v_0(t), \tag{23}$$

then, one has $\dot{\tilde{P}}(t) = \tilde{V}(t)$. Thus, the global switching function $S(t)$ in (18) can be rewritten as

$$S(t) = k_1 L_H \tilde{P}(t) + k_2 L_H \tilde{V}(t). \tag{24}$$

The Lyapunov candidate function is chosen as

$$V_\epsilon(t) = \frac{1}{2}\tilde{P}^{\mathrm{T}}(t)\tilde{P}(t), \tag{25}$$

and one has

$$\dot{V}_\epsilon(t) = \tilde{P}^{\mathrm{T}}(t)\dot{\tilde{P}}(t) = \tilde{P}^{\mathrm{T}}(t)\tilde{V}(t). \tag{26}$$

On the sliding surface $S(t) = \mathbf{0}$, one has

$$k_1 L_H \tilde{P}(t) + k_2 L_H \tilde{V}(t) = \mathbf{0}. \tag{27}$$

Considering the invertibility of L_H, the derivative of $V_\epsilon(t)$ can be written as,

$$\begin{aligned}\dot{V}_\epsilon(t) =& -\frac{k_1}{k_2}\tilde{P}^{\mathrm{T}}(t)\tilde{P}(t)\\ \leq& -\frac{2k_1}{k_2}V_\epsilon(t).\end{aligned} \tag{28}$$

According to Lyapunov stability theory, one has $\lim_{t\to\infty} V_\epsilon(t) = \mathbf{0}$, then it can be obtained that $\lim_{t\to\infty} \tilde{P}(t) = \mathbf{0}$. Furthermore, it yields that $\lim_{t\to\infty} \tilde{V}(t) = \mathbf{0}$. Thus, one has

$$\lim_{t\to\infty} \|x_i(t) - f_i(t) - x_0(t)\| = 0. \tag{29}$$

According to Definition 1, it can be obtained that the multi-UAV system (12) achieves the desired formation tracking and the formation tracking error boundary is $\sigma_f = 0$. The proof is completed. □

The sliding mode control objective is to make each follower UAV i reach the sliding mode surface $s_i(t) = 0$ and remain on it. Therefore, from Lemma 3, the formation tracking problem is transformed to a sliding mode control problem. Then we will design the formation tracking protocol based on sliding mode control approach in continuous-time form.

4. Continuous formation tracking protocol design

The distributed formation tracking protocol for follower UAV i $(i = 1, 2, \ldots, N)$ is proposed as

$$\begin{aligned}u_i(t) =& (KB(d_i + a_{i0}))^{-1}\Bigg(KB\sum_{j=1, j\neq i}^{N} a_{ij}u_j(t) - \Big[KA\big((d_i + a_{i0})x_i(t)\\ &- \sum_{j=1, j\neq i}^{N} a_{ij}x_j(t)\big) - a_{i0}KAx_0(t) - a_{i0}KBu_{\min} + \rho\,\mathrm{sgn}(s_i(t))\\ &- K\big((d_i + a_{i0})\dot{f}_i(t) - \sum_{j=1, j\neq i}^{N} a_{ij}\dot{f}_j(t)\big)\Big]\Bigg),\end{aligned} \tag{30}$$

where $d_i = \sum_{j=1, j\neq i}^{N} a_{ij}$, ρ is a control parameter.

Theorem 1. *Under protocol (30), the multi-UAV system (12) can achieve the desired formation tracking with the error boundary $\sigma_f = 0$ if the matrix $K = [k_1, k_2]$ satisfies $k_1 > 0$, $k_2 > 0$, and the control parameter $\rho > 0$.*

Proof. It holds from (18) that

$$\dot{S}(t) = (L_H \otimes K)(\dot{X}(t) - \dot{F}(t)) - (H \otimes K)(\mathbf{1}_N \otimes \dot{x}_0(t)). \tag{31}$$

Substituting $\dot{x}_0(t)$ and $\dot{X}(t)$ by the system equations of leader and followers yields

$$\begin{aligned}\dot{S}(t) =& (L_H \otimes K)((I_N \otimes A)X(t) + (I_N \otimes B)U(t)) - (L_H \otimes K)\dot{F}(t)\\ &- (H \otimes K)\big(\mathbf{1}_N \otimes (Ax_0(t) + Bu_0(t))\big).\end{aligned} \tag{32}$$

Let $U(t) = [u_1(t), u_2(t), \ldots, u_N(t)]^{\mathrm{T}}$, the protocols for followers can be rewritten in the following compact form

$$\begin{aligned}U(t) =& -\big(L_H \otimes (KB)\big)^{-1}\Big((L_H \otimes KA)X(t) - H_{\mathbf{1}} \otimes (KAx_0(t) + KBu_{\min})\\ &+ \rho\,\mathrm{sgn}(S(t)) - (L_H \otimes K)\dot{F}(t)\Big).\end{aligned} \tag{33}$$

Substituting the control input (33) into (32), the equation of $\dot{S}(t)$ gives

$$\dot{S}(t) = -\rho\,\mathrm{sgn}(S(t)) - H_{\mathbf{1}} \otimes (KB(u_0(t) - u_{\min})). \tag{34}$$

For each UAV i, one has from (34) that

$$\dot{s}_i(t) = -\rho\,\mathrm{sgn}(s_i(t)) - a_{i0}KB(u_0(t) - u_{\min}). \tag{35}$$

Choose the Lyapunov candidate function for UAV i as

$$V_{is}(t) = \frac{1}{2}s_i(t)^2, \tag{36}$$

which means that

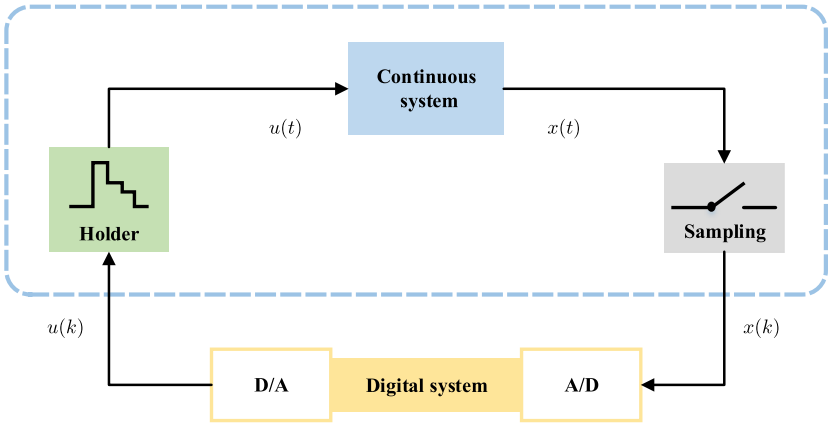

Fig. 4. Processing of digital system for continuous system.

$$\dot{V}_{is}(t) = s_i(t)\dot{s}_i(t). \tag{37}$$

Since

$$-(u_0(t) - u_{\min}) \leq 0, \tag{38}$$

one has $\dot{s}_i(t) \leq -\rho\,\mathrm{sgn}(s_i(t))$. Thus,

$$\begin{aligned} \dot{V}_{is}(t) &= s_i(t)\dot{s}_i(t) \\ &\leq s_i(t)(-\rho\,\mathrm{sgn}(s_i(t))) \\ &\leq -\rho|s_i(t)| \\ &\leq -\sqrt{2}\rho(V_{is}(t))^{\frac{1}{2}}. \end{aligned} \tag{39}$$

According to Lemma 2, for each UAV i, it can reach the sliding surface $s_i(t) = 0$ in a finite time and keep on it. It means that for the multi-UAV system (12), it can reach the sliding surface $S(t) = \mathbf{0}$ in a finite time and remain on it. From Lemma 3, it can be concluded that the multi-UAV system (12) achieves the desired formation tracking and the error boundary is $\sigma_f = 0$. The proof is completed. □

According to Theorem 1, a feasible procedure to construct the continuous time-varying formation tracking protocol is given in Algorithm 1.

Algorithm 1 Procedure to construct the continuous time-varying formation tracking protocol.

1: **for** each follower UAV i ($i = 1, 2, \ldots, N$), **do**
2: Choose the desired continuous time-varying formation $f_i(t) = [f_{ip}(t), f_{iv}(t)]^{\mathrm{T}}$;
3: **if** the condition $\dot{f}_{ip}(t) = f_{iv}(t)$ is met, **then**
4: Determine the $u_{\min}$ based on the movement state of the leader;
5: Select an appropriate coefficient matrix $K = [k_1, k_2]$ with $k_1 > 0$ and $k_2 > 0$;
6: Choose appropriate $\rho > 0$;
7: Complete the construct of the formation tracking protocol shown in (30);
8: **end if**
9: **end for**

5. Discrete formation tracking protocol design

In the above section, the formation tracking protocol under the continuous-time model is given. However, in industrial systems, digital systems can only handle sampled signals, not continuous signals. The processing flow of the digital system for continuous system is shown in Fig. 4. It means that the above continuous-time control protocol cannot be directly applied to the engineering field. Therefore, in this section, we will construct the formation tracking controller in a discrete-time form.

Before designing a discrete-time formation tracking protocol, a discrete-time system model should be first established. Substituting the derivative by the forward difference, the UAV i ($i = 0, 1, 2, \ldots, N$) in (11) can be discretized as

$$x_i(k+1) = \bar{A}x_i(k) + \bar{B}u_i(k), \tag{40}$$

where k represents the time $t = kT$, $x_i(k) = [p_i(k), v_i(k)]^{\mathrm{T}} \in \mathbb{R}^2$,

$$\bar{A} = \begin{bmatrix} 1 & T \\ 0 & 1 \end{bmatrix}, \ \bar{B} = \begin{bmatrix} 0 \\ T \end{bmatrix},$$

and T is the sampling period.

Similarly, the discrete multi-UAV system of N followers can be written as

$$X(k+1) = (I_N \otimes \bar{A})X(k) + (I_N \otimes \bar{B})U(k). \tag{41}$$

The following definition is given to describe the sliding mode characteristics of the discrete sliding mode controller.

Definition 2. [42] For all $i = 1, 2, \ldots, N$, the discrete system (40) is said to be in a quasi-sliding mode (QSM) in the Δ vicinity of the switching function $s_i(k)$ if the motion of system (40) met

$$\{x_i(k) : \|s_i(k) = K\epsilon_i(k)\| \le \Delta, \forall k > k^*\}, \tag{42}$$

where Δ is a positive constant and k^* is a positive integer. The specified space domain defined by $-\Delta$ and Δ is called a quasi-sliding mode domain (QSMD), and Δ is named the width of the QSMD.

Remark 3. For the discrete-time case, the discrete sliding mode controller is in a QSM, while as shown in Lemma 3, the continuous sliding mode controller is in an ideal quasi-sliding mode (IQSM) with $\Delta = 0$. It means that the motion of the discrete sliding mode system is not as smooth as the continuous system.

Lemma 4. *For the multi-UAV system (40), if the switching function $s_i(k)$ is in a QSBD with width Δ, then the desired formation tracking will be achieved with an error boundary $\sigma_f \le \frac{\|L_H^{-1}\|}{(k_1+k_2)\sqrt{2}}\Delta$.*

Proof. From the proof process of Lemma 3, it holds

$$S(k) = k_1 L_H \tilde{P}(k) + k_2 L_H \tilde{V}(k), \tag{43}$$

and considering the invertibility of L_H, one has

$$L_H^{-1} S(k) = k_1 \tilde{P}(k) + k_2 \tilde{V}(k). \tag{44}$$

Then taking the norm in both side yields

$$\begin{aligned} k_1\|\tilde{P}(k)\| + k_2\|\tilde{V}(k)\| &= \|L_H^{-1}S(k)\| \\ &\le \|L_H^{-1}\|\|S(k)\|. \end{aligned} \tag{45}$$

Suppose that the position and velocity error boundaries are equal. Since the formation tracking error boundary is σ_f, one has $\|\tilde{P}(k)\| = \|\tilde{V}(k)\| = \sqrt{\frac{N}{2}}\sigma_f$, then it follows

$$(k_1 + k_2)\sqrt{\frac{N}{2}}\sigma_f \le \|L_H^{-1}\|\sqrt{N}\Delta. \tag{46}$$

It can be obtained that

$$\sigma_f \le \frac{\|L_H^{-1}\|}{(k_1 + k_2)\sqrt{2}}\Delta. \tag{47}$$

The proof is completed. □

The distributed discrete-time formation tracking protocol for follower UAV i $(i = 1, 2, ..., N)$ is proposed as

$$\begin{aligned} u_i(k) =& (K\bar{B}(d_i + a_{i0}))^{-1}\Bigg(K\bar{B}\sum_{j=1, j\neq i}^{N} a_{ij}u_j(k) - \Big[K\bar{A}\Big((d_i + a_{i0})x_i(k) - \sum_{j=1, j\neq i}^{N} a_{ij}x_j(k)\Big) \\ &- a_{i0}K\bar{A}x_0(k) - a_{i0}K\bar{B}\tilde{u}_{i0}(k) + (qT - 1)s_i(k) + \varepsilon T\,\mathrm{sgn}(s_i(k)) \\ &- K\Big((d_i + a_{i0})f_i(k+1) - \sum_{j=1, j\neq i}^{N} a_{ij}f_j(k+1)\Big)\Big]\Bigg), \end{aligned} \tag{48}$$

where ε and q are two control parameters, $\tilde{u}_{i0}(k) = \tilde{u}_1 - \tilde{u}_2\,\mathrm{sgn}(s_i(k))$, $\tilde{u}_1 = (u_{\max} + u_{\min})/2$, and $\tilde{u}_2 = (u_{\max} - u_{\min})/2$.

Remark 4. It should be noted that in the discrete-time formation tracking protocol (48), both the upper and lower bounds of the leader's acceleration, namely, $u_{\max}$ and $u_{\min}$, are required. In contrast, only the lower bound $u_{\min}$ in the continuous-time protocol (30) is needed. It means that compared with the continuous-time case, more information about the leader's control input should be known in the discrete-time case.

Theorem 2. *Under protocol (48), if the control parameters satisfy $\varepsilon > 0$, $q > 0$, and $1 - qT > 0$, then the discrete-time multi-UAV system (40) can realize the expected formation tracking where the width of QSMD is $\Delta = \max\{\Delta_1, \Delta_2\}$ with*

$$\Delta_1 = \frac{\varepsilon T + a_{i0} K \bar{B}(u_{\max} - u_{\min}) + \eta_0}{2 - qT}, \eta_0 > 0, \tag{49}$$

and

$$\Delta_2 = \varepsilon T + a_{i0} K \bar{B}(u_{\max} - u_{\min}). \tag{50}$$

In addition, the formation tracking error boundary is $\sigma_f \leq \frac{\|L_H^{-1}\|}{(k_1+k_2)\sqrt{2}}\Delta$.

Proof. It holds from (18) that

$$S(k+1) = (L_H \otimes K)(X(k+1) - F(k+1)) - (H \otimes K)(\mathbf{1}_N \otimes x_0(k+1)). \tag{51}$$

Substituting $x_0(k+1)$ and $X(k+1)$ with the system equations of the leader and followers yields

$$\begin{aligned} S(k+1) =& (L_H \otimes K)((I_N \otimes \bar{A})X(k) + (I_N \otimes \bar{B})U(k)) \\ & - (H \otimes K)\big(\mathbf{1}_N \otimes (\bar{A}x_0(k) + \bar{B}u_0(k))\big) \\ & - (L_H \otimes K)F(k+1). \end{aligned} \tag{52}$$

Note $U(k) = [u_1(k), u_2(k), \ldots, u_N(k)]^{\mathrm{T}}$, the discrete-time protocols for followers can be rewritten in the following compact form

$$\begin{aligned} U(k) =& -\big(L_H \otimes (K\bar{B})\big)^{-1}\Big((L_H \otimes K\bar{A})X(k) - H_{\mathbf{1}} \otimes (K\bar{A}x_0(k)) - (H \otimes K\bar{B})\tilde{U}_0(k) \\ & + (qT-1)S(k) + \varepsilon T \operatorname{sgn}(S(k)) - (L_H \otimes K)F(k+1)\Big), \end{aligned} \tag{53}$$

where $\tilde{U}_0(k) = \mathbf{1}_N \otimes \tilde{u}_{i0}(k)$.

Substituting the control input (53) into (52), the equation of $S(k+1)$ gives

$$S(k+1) = (1 - qT)S(k) - H_{\mathbf{1}} \otimes (K\bar{B}u_0(k)) + (H \otimes K\bar{B})\tilde{U}_0(k) - \varepsilon T \operatorname{sgn}(S(k)). \tag{54}$$

For each UAV i, it follows from (54) that

$$s_i(k+1) = (1 - qT)s_i(k) - \varepsilon T \operatorname{sgn}(s_i(k)) - a_{i0} K \bar{B}(u_0(k) - \tilde{u}_{i0}(k)), \tag{55}$$

where $\tilde{u}_{i0}(k) = \tilde{u}_1 - \tilde{u}_2 \operatorname{sgn}(s_i(k))$.

Choose the Lyapunov candidate function for UAV i as

$$V_{si}(k) = s_i(k)^2, \tag{56}$$

which means that

$$\begin{aligned} \delta V_{si}(k) &= V_{si}(k+1) - V_{si}(k) \\ &= (s_i(k+1) + s_i(k))(s_i(k+1) - s_i(k)). \end{aligned} \tag{57}$$

Then let us discuss the cases $s_i(k) \geq \Delta_1$, $s_i(k) \leq -\Delta_1$, $0 < s_i(k) < \Delta_1$, and $-\Delta_1 < s_i(k) < 0$.

Case 1: $s_i(k) \geq \Delta_1$. From (55), one gets

$$\begin{aligned} s_i(k+1) - s_i(k) &= -a_{i0} K \bar{B}(u_0(k) - u_{\min}) - \varepsilon T - qT s_i(k) \\ &\leq -\varepsilon T - qT s_i(k), \end{aligned} \tag{58}$$

and

$$\begin{aligned} s_i(k+1) + s_i(k) &= -a_{i0} K \bar{B}(u_0(k) - u_{\min}) + (2 - qT)s_i(k) - \varepsilon T \\ &\geq a_{i0} K \bar{B}(u_{\max} - u_0(k)) + \eta_0. \end{aligned} \tag{59}$$

Then, one has

$$\begin{aligned} \delta V_{si}(k) &\leq \{a_{i0} K \bar{B}(u_{\max} - u_0(k)) + \eta_0\}(-\varepsilon T - qT s_i(k)) \\ &\leq -\eta_0 \varepsilon T - \eta_0 qT s_i(k) \\ &\leq -\eta_0 \varepsilon T - \eta_0 qT \Delta_1. \end{aligned} \tag{60}$$

Case 2: $s_i(k) \leq -\Delta_1$. From (55), one gets

$$\begin{aligned} s_i(k+1) - s_i(k) &= -a_{i0} K \bar{B}(u_0(k) - u_{\max}) + \varepsilon T - qT s_i(k) \\ &\geq \varepsilon T - qT s_i(k), \end{aligned} \tag{61}$$

and

$$\begin{aligned} s_i(k+1)+s_i(k) &= -a_{i0}K\bar{B}(u_0(k)-u_{\max})+(2-qT)s_i(k)+\varepsilon T \\ &\le a_{i0}K\bar{B}(u_{\min}-u_0(k))-\eta_0. \end{aligned} \tag{62}$$

Then, one has

$$\begin{aligned} \delta V_{si}(k) &\le \{a_{i0}K\bar{B}(u_{\min}-u_0(k))-\eta_0\}(\varepsilon T-qTs_i(k)) \\ &\le -\eta_0\varepsilon T+\eta_0 qTs_i(k) \\ &\le -\eta_0\varepsilon T-\eta_0 qT\Delta_1. \end{aligned} \tag{63}$$

From the analyses of Case 1 and 2, one can see that $V_{si}(k)$ is decreasing at a rate greater than $-\eta_0\varepsilon T-\eta_0 qT\Delta_1$ per step when $s_i(k)$ is outside of the band, namely, $s_i(k)\ge\Delta_1$ or $s_i(k)\le-\Delta_1$. Then it can be obtained that $s_i(k)$ will decrease to the region defined by Δ_1 in finite steps. Thus, for the boundary $\Delta=\max\{\Delta_1,\Delta_2\}$, one can obtain that $s_i(k)$ will decrease to the region defined by Δ in finite steps.

Case 3: $0<s_i(k)<\Delta_1$. From (55), one gets

$$s_i(k+1)=-a_{i0}K\bar{B}(u_0(k)-u_{\min})-\varepsilon T+(1-qT)s_i(k), \tag{64}$$

and then one has

$$\begin{aligned} s_i(k+1) &> -a_{i0}K\bar{B}(u_0(k)-u_{\min})-\varepsilon T \\ &> -\Delta_2. \end{aligned} \tag{65}$$

Case 4: $-\Delta_1<s_i(k)<0$. From (55), one gets

$$s_i(k+1)=-a_{i0}K\bar{B}(u_0(k)-u_{\max})+\varepsilon T+(1-qT)s_i(k), \tag{66}$$

and then one has

$$\begin{aligned} s_i(k+1) &< a_{i0}K\bar{B}(u_{\max}-u_0(k))+\varepsilon T \\ &< \Delta_2. \end{aligned} \tag{67}$$

From the analyses of Case 3 and 4, one can get that when $|s_i(k)|<\Delta_1$, $|s_i(k+1)|<\Delta_2$. Thus, for the boundary $\Delta=\max\{\Delta_1,\Delta_2\}$, one can obtain that when $|s_i(k)|<\Delta$, $|s_i(k+1)|<\Delta$.

According to the above analysis of the four cases, it can be concluded that the switching function $s_i(k)$ has a ultimate bounded stability with boundary Δ, namely $s_i(k)$ is in a QSM with width Δ. Then from Lemma 4, it can be obtained that the desired formation tracking can be achieved and the formation tracking error boundary is $\sigma_f\le\frac{\|L_H^{-1}\|}{(k_1+k_2)\sqrt{2}}\Delta$. The proof is completed. □

Remark 5. Under the continuous protocol, the continuous-time system is uniformly asymptotically stable. However, the discrete-time system is bounded stable under the discrete protocol. It means that the transition from continuous-time to discrete-time model weakens the stability of the system. The stability conditions of the system become more stringent and are related to the sampling time.

According to Theorem 2, a feasible procedure to construct the discrete time-varying formation tracking protocol is given in Algorithm 2.

Algorithm 2 Procedure to construct the discrete time-varying formation tracking protocol.

```
for each follower UAV i (i = 1, 2, ..., N), do
    Choose the desired discrete time-varying formation f_i(k) = [f_ip(k), f_iv(k)]^T;
    Determine the u_min and u_max based on the movement state of the leader;
    Select a common sample time T;
    if the condition f_ip(k+1) − f_ip(k) = T f_iv(k) is met, then
        Select an appropriate coefficient matrix K = [k_1, k_2] with k_1 > 0 and k_2 > 0;
        Choose appropriate q > 0 and ε > 0;
        if 1 − qT ≤ 0 then
            back to Step 4;
        end if
        Complete the construct of the formation tracking protocol shown in (48);
    end if
end for
```

6. Experiment results

In order to verify the theoretical results, virtual experiments with UAVs are conducted. In this section, the multiple UAV formation tracking simulation platform will be introduced, experiments with six UAVs using the proposed sliding mode formation tracking protocol will be performed, and the analysis of the experimental results will be given. The virtual experiment video can be found on https://youtu.be/dHqNoYIUqD8 and https://www.bilibili.com/video/BV19y4y1r7RZ/.

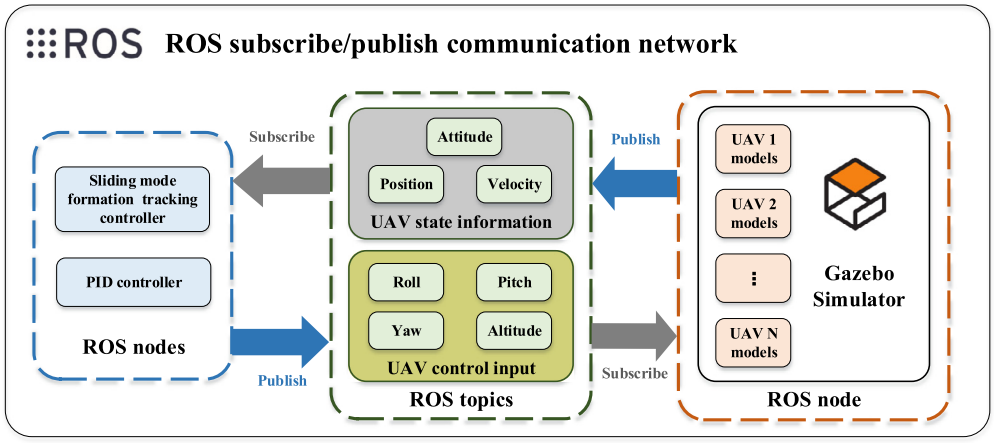

Fig. 5. Structure of the formation tracking platform.

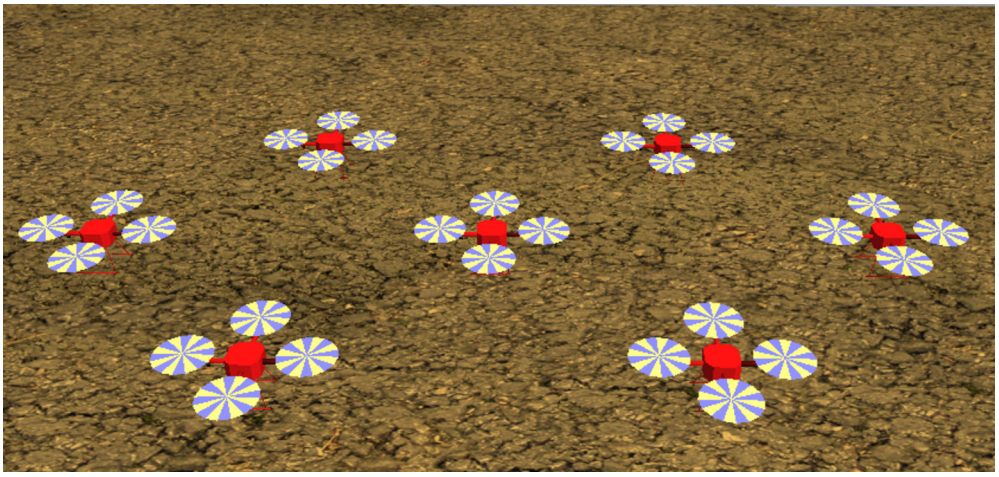

Fig. 6. Quadrotor UAV used in the formation tracking platform.

6.1. Experiment platform

In order to establish the virtual experiment as close as possible to the reality, Robot Operating System (ROS) and Gazebo simulator are used to create the multiple-UAV formation tracking virtual experiment platform. ROS is a collection of software frameworks for robot software development and provides services designed for a heterogeneous computer cluster such as hardware abstraction, low-level device control, etc. As a well-designed open source 3D robotics simulator, Gazebo can use multiple high-performance physics engines, such as ODE, Bullet, etc. A multi-UAV virtual experiment environment can be constructed in Gazebo, where the gravity, friction, contact forces, and the other physical parameters are considered. By integrating with ROS, Gazebo simulator has become a de facto standard in robotics research.

Message-passing between processes is the main functionality of the ROS communication network. A node is a single process running in ROS. Topics are named buses over which nodes send and receive messages. In the formation tracking platform, the Gazebo simulator, the formation tracking controller, and the PID controller are three typical nodes. The UAV state information and control inputs are two typical topics. The workflow of the entire formation tracking platform is as follows. First, Gazebo sends states information such as position, velocity, and attitude of each UAV through ROS topics. Then, the sliding mode formation tracking controller and PID controller nodes subscribe to the states of UAVs, calculate the control inputs of pitch, roll, yaw, and altitude channels of UAVs, and then publish them to the corresponding ROS topic. Finally, Gazebo simulates the movement of UAVs according to their control inputs, displays the trajectories of UAVs in real time, and updates the states of UAVs. The whole structure of the formation tracking virtual experiment platform is shown in Fig. 5. (See also Fig. 6.)

6.2. Experiment results

A multi-UAV system with one leader and six followers is considered. As indicated in Fig. 7, the control of yaw and altitude direction is through with PID controller. The X and Y directions, namely, roll and pitch channels are controlled by the sliding mode formation tracing controller. As for the design of the formation tracking controller in X and Y directions, the state $x_i(t)$, formation vector $f_i(t)$, and control input $u_i(t)$ of UAV i can be rewritten as $x_i(t) = [p_{iX}(t), v_{iX}(t), p_{iY}(t), v_{iY}(t)]^{\mathrm{T}}$, $f_i(t) = [f_{ipX}(t), f_{ivX}(t), f_{ipY}(t), f_{ivY}(t)]^{\mathrm{T}}$, and $u_i(t) = [u_{iX}(t), u_{iY}(t)]^{\mathrm{T}}$, respectively. The interaction topology with 0-1 weights among the UAVs is shown in Fig. 8. One can verify that there exists a directed spanning tree from the leader. Then one has that $H = \mathrm{diag}(1, 0, 0, 0, 0, 0)$, and

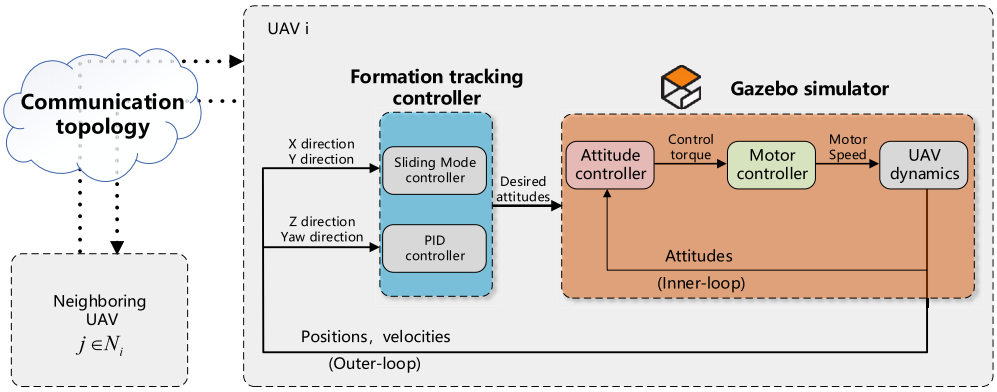

Fig. 7. Block diagram of the proposed formation control scheme.

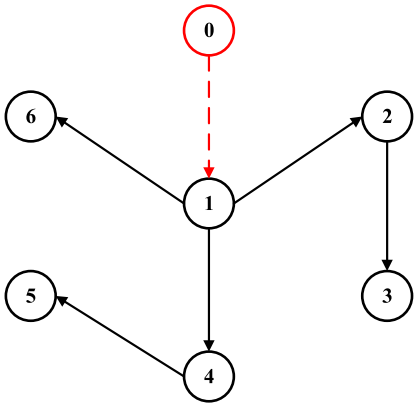

Fig. 8. Interaction topology among seven UAVs.

$$L = \begin{bmatrix} 0 & 0 & 0 & 0 & 0 & 0 \\ -1 & 1 & 0 & 0 & 0 & 0 \\ 0 & -1 & 1 & 0 & 0 & 0 \\ -1 & 0 & 0 & 1 & 0 & 0 \\ 0 & 0 & 0 & -1 & 1 & 0 \\ -1 & 0 & 0 & 0 & 0 & 1 \end{bmatrix}.$$

The leader makes a circular motion around the origin of the coordinates, where $w_L = 0.157$ rad/s and $r_L = 20$ m. Then, one can choose that $u_{\min} = -1$ and $u_{\max} = 1$. The desired time-varying formation for the followers is a circular motion with radius $r = 10$ m, angular velocity $\omega = 0.314$ rad/s, and the phase difference $\pi/3$. The corresponding formation vector $f_i(t)$ is

$$f_i(t) = \begin{bmatrix} r\cos(\omega t + \frac{(i-1)\pi}{3}) \\ -\omega r \sin(\omega t + \frac{(i-1)\pi}{3}) \\ r\sin(\omega t + \frac{(i-1)\pi}{3}) \\ \omega r \cos(\omega t + \frac{(i-1)\pi}{3}) \end{bmatrix}, i = 1, 2, \ldots, 6.$$

The following formation tracking error function $\sigma_F(t)$ for the whole multi-UAV system is defined to measure the achievement degree of the time-varying formation tracking

$$\sigma_F(t) = \|X(t) - F(t) - \mathbf{1}_N \otimes x_0(t)\|. \tag{68}$$

Both continuous-time and discrete-time formation tracking controllers are applied in the virtual experiments. Matrix $K = I_2 \otimes [3, 1]$ is chosen for the design of switching function. According to Theorem 1, the parameter of continuous protocol (30) is $\rho = 0.05$; according to Theorem 2, the parameters of discrete protocol are chosen as $\varepsilon = 0.05$ and $q = 4.5$. Experiment 1 is conducted to verify the effectiveness of continuous formation tracking protocol. Experiment 2 and 3 are performed to demonstrate the effect of sampling time T on the performance of discrete formation tracking protocol with $T = 0.05$ s and $T = 0.2$ s, respectively.

6.2.1. Experiment 1

Continuous protocol is used in this experiment (Fig. 9). Fig. 10 shows the trajectories of seven UAVs in X-Y plane within 40 s, where the positions of UAVs at $t = 0$ s and $t = 40$ s are represented by round and hexagon markers, respectively. The positions of UAVs in X-Y plane at $t = 40$ s are indicated in Fig. 11. The angles of pitch θ and roll ϕ of follower 1 are shown in Fig. 12. The yaw angle ψ and switching

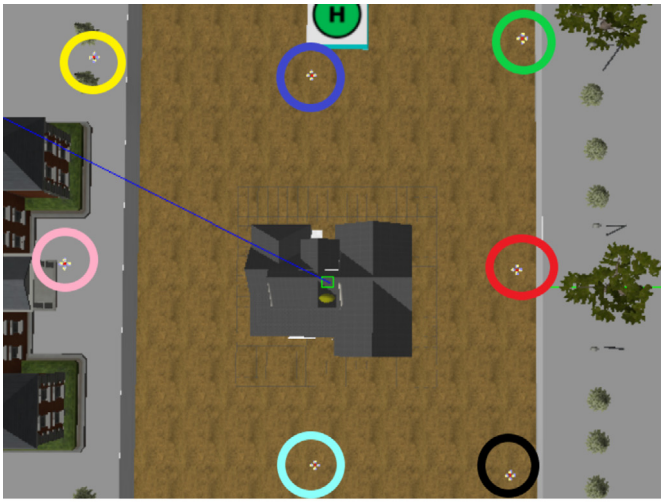

(a) t=0s

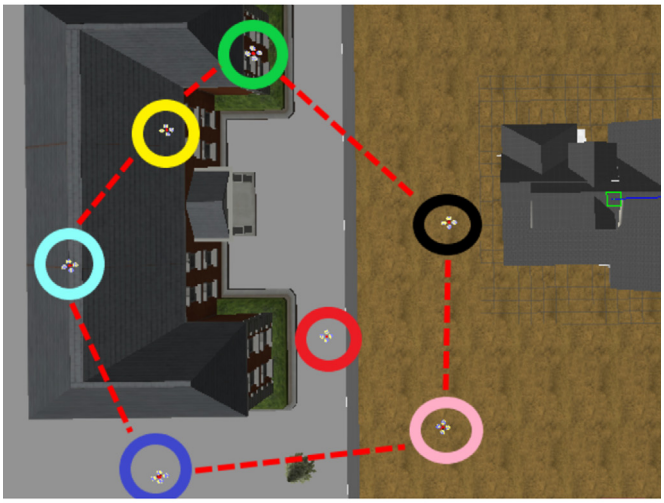

(b) t=10s

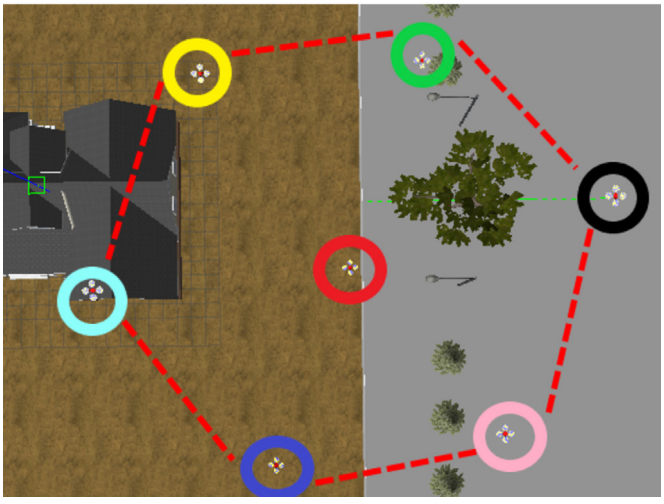

(c) t=20s

Fig. 9. Seven UAVs during the formation tracking in experiment 1 in Gazebo at different time.

functions $s_1(t)$ of follower 1 are represented in Fig. 13 and Fig. 14, respectively. Since the attitude angles and switching functions of the other followers are similar to those of follower 1, only follower 1 is shown as an example. The formation tracking error function $\sigma_F(t)$ for the whole multi-UAV system is indicated in Fig. 15.

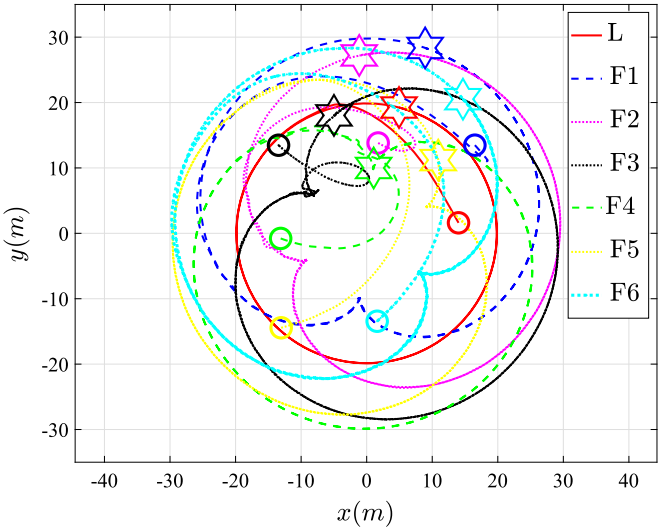

Fig. 10. Trajectories in X-Y plane of seven UAVs within 40 s in experiment 1.

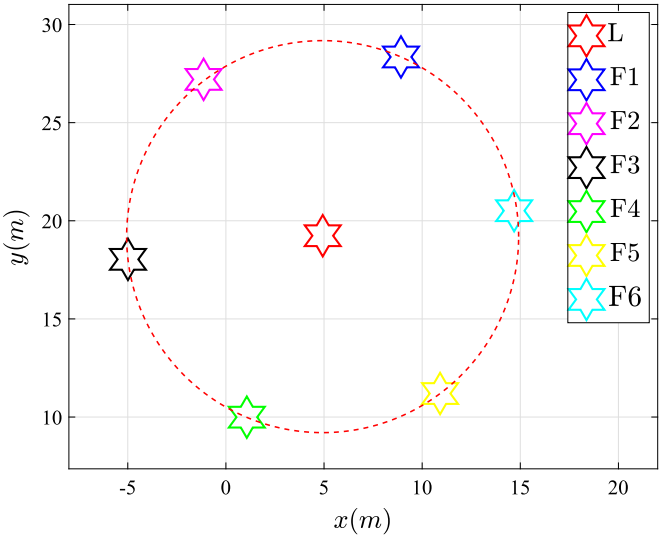

Fig. 11. Positions of seven UAVs at 40 s in experiment 1.

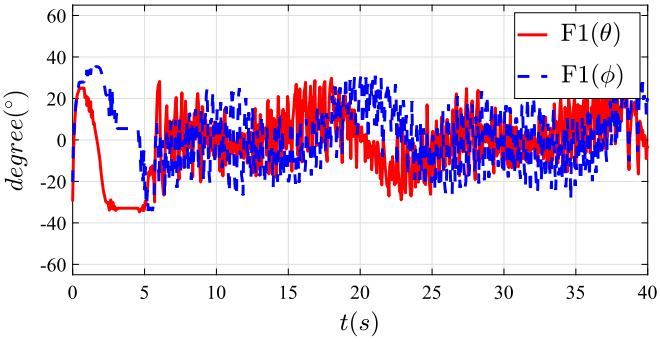

Fig. 12. Pitch θ and roll ϕ angles of follower 1 within 40 s in experiment 1.

According to the red circle in Fig. 11, the six followers reach exactly on the circumference of the circle with $r = 10$ m at $t = 40$ s, and the leader is at the center of the circle. One can see that the desired circular formation with $r = 10$ m among followers is achieved. Therefore, it can be concluded that the desired time-varying formation tracking is realized.

6.2.2. Experiment 2

Discrete protocol with sample time $T = 0.05$ s is used in this experiment. The trajectories of seven UAVs in X-Y plane within 40 s are shown in Fig. 16. The positions of UAVs in X-Y plane at $t = 40$ s are indicated in Fig. 17. (See also Figs. 18 and 19.) The switching functions $s_1(t)$ of follower 1 are represented in Fig. 20 and the formation tracking error function $\sigma_F(k)$ is indicated in Fig. 21.

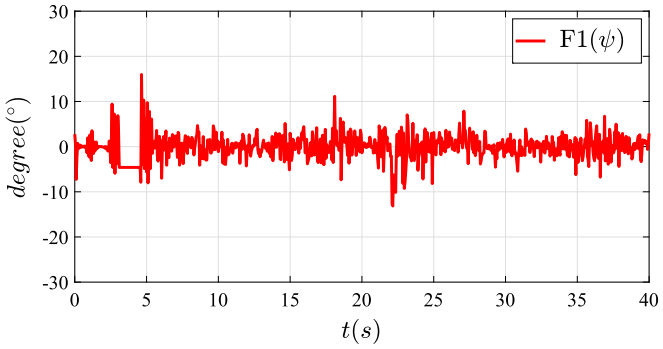

Fig. 13. Yaw ψ angle of follower 1 within 40 s in experiment 1.

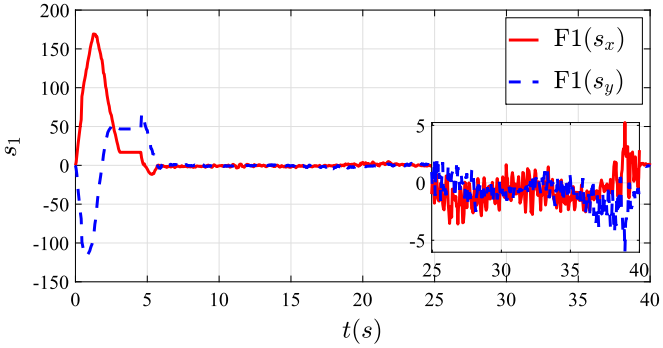

Fig. 14. Switching function $s_1(t)$ of follower 1 within 40 s in experiment 1.

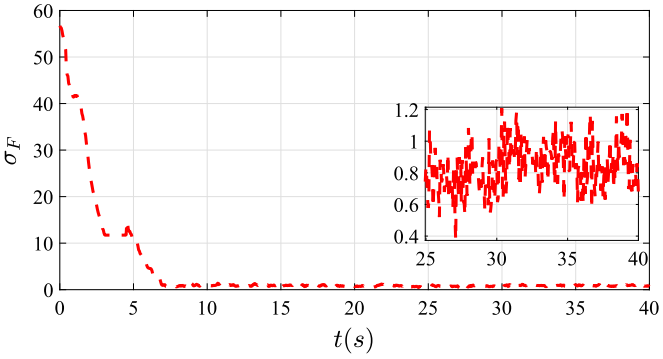

Fig. 15. Formation tracking error $\sigma_F(t)$ within 40 s in experiment 1.

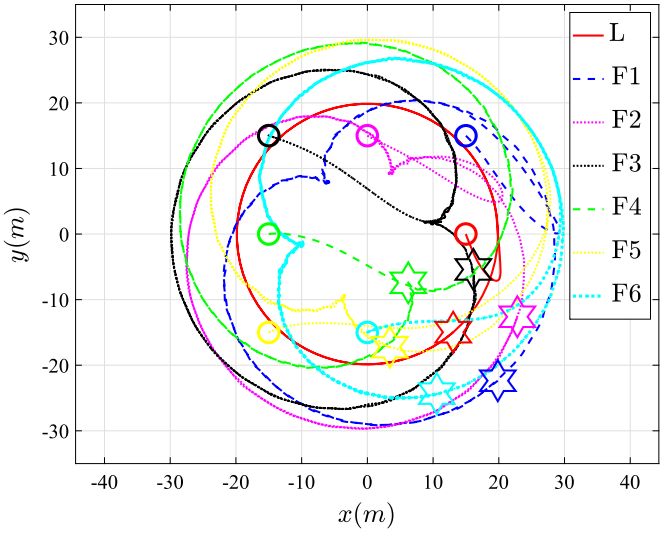

Fig. 16. Trajectories in X-Y plane of seven UAVs within 40 s in experiment 2.

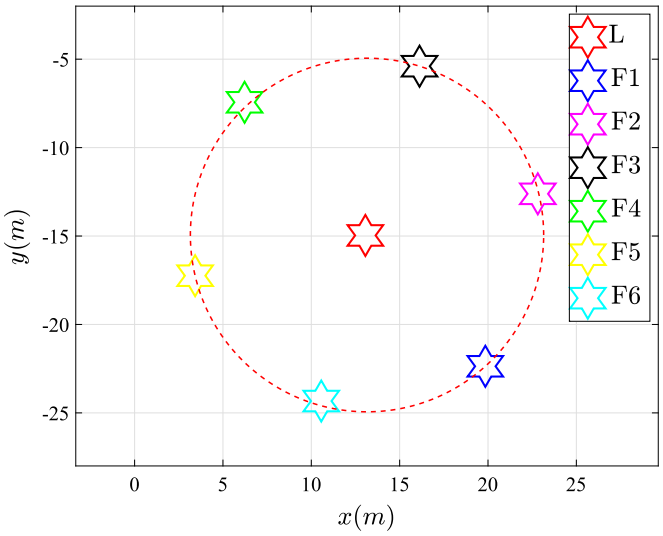

Fig. 17. Positions of seven UAVs at 40 s in experiment 2.

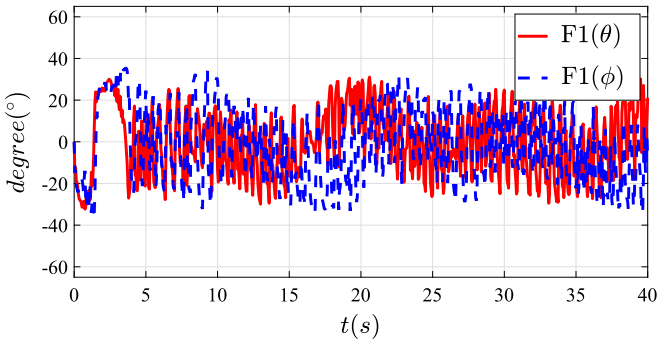

Fig. 18. Pitch θ and roll ϕ angles of follower 1 within 40 s in experiment 2.

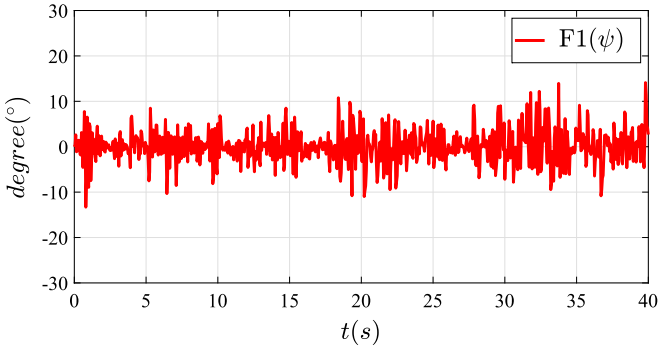

Fig. 19. Yaw ψ angle of follower 1 within 40 s in experiment 2.

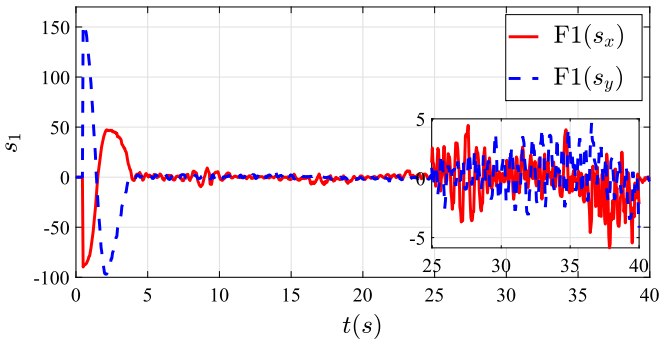

Fig. 20. Switching function $s_1(k)$ of follower 1 within 40 s in experiment 2.

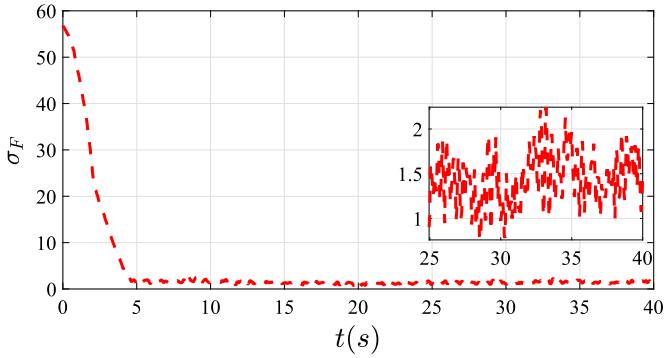

Fig. 21. Formation tracking error $\sigma_F(k)$ within 40 s in experiment 2.

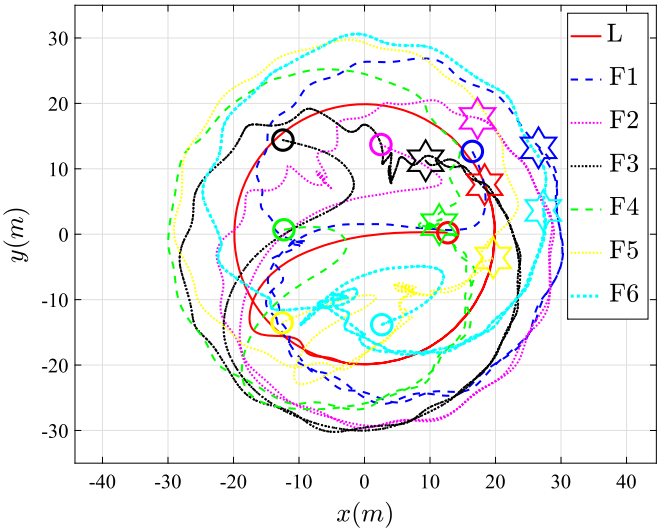

Fig. 22. Trajectories in X-Y plane of seven UAVs within 40 s in experiment 3.

Table 1
Comparisons for different formation tracking controllers.

Experiment	Formation tracking controllers	Control parameters	Mean value of $\sigma_F(t)$ with $t \in [25, 40]$ s
1	Continuous controller	$\rho = 0.05$	0.8397
2	Discrete controller with $T = 0.05$ s	$\varepsilon = 0.05$, $q = 4.5$	1.4405
3	Discrete controller with $T = 0.2$ s		4.5250

From the red circle in Fig. 17, the six followers reach exactly on the circumference of the circle with $r = 10$ m at $t = 40$ s, and the leader is at the center of the circle. One can see that the desired circular formation with $r = 10$ m among followers is achieved. In addition, from Fig. 20 and Fig. 21, it can be seen that the switching function and formation tracking error function decrease rapidly at the beginning and eventually converge to a bounded region, which is coincident with the conclusion of bounded stability given in Theorem 2. Thus, it can be obtained that the expected time-varying formation tracking is achieved.

6.2.3. Experiment 3

Discrete protocol with sample time $T = 0.2$ s is used in this experiment. The trajectories of seven UAVs in X-Y plane within 40 s are shown in Fig. 22. The positions of UAVs in X-Y plane at $t = 40$ s are indicated in Fig. 23. (See also Figs. 24 and 25.) The switching functions $s_1(k)$ of follower 1 are represented in Fig. 26 and the formation tracking error function $\sigma_F(k)$ is indicated in Fig. 27. From Fig. 22 and Fig. 23, one can see that the desired circular formation with $r = 10$ m among followers is achieved. In addition, from Fig. 26 and Fig. 27, it can be seen that the switching function $s_1(k)$ and formation tracking error function $\sigma_F(k)$ converge eventually to a bounded region. Therefore, it can be concluded that the desired time-varying formation tracking is realized.

6.2.4. Summary

The control parameters and formation errors of three experiments are shown in Table 1. Comparing Experiment 2 with Experiment 3, one can see that as the sampling time T increases, the upper bounds of convergence of switching function and formation error also increase, which is consistent with the expression of QSMD width given in Theorem 2. The results of Experiment 1 can be considered as a discrete controller with the sampling time tending to 0. However, considering the fact that Gazebo is a simulator with physics engines, and the continuous control inputs are converted to sampled signal to process in Gazebo, the formation tracking error σ_F is not zero. Thus, it can be concluded that the accuracy of time-varying formation tracking is improved as the sampling time T decreases.

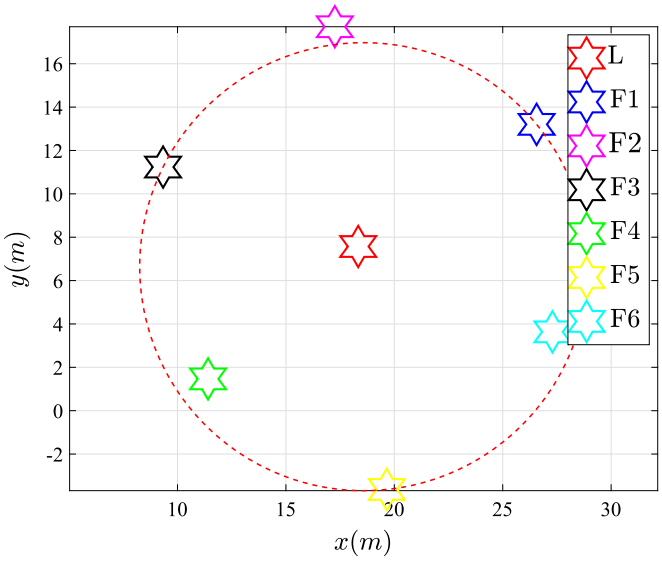

Fig. 23. Positions of seven UAVs at 40 s in experiment 3.

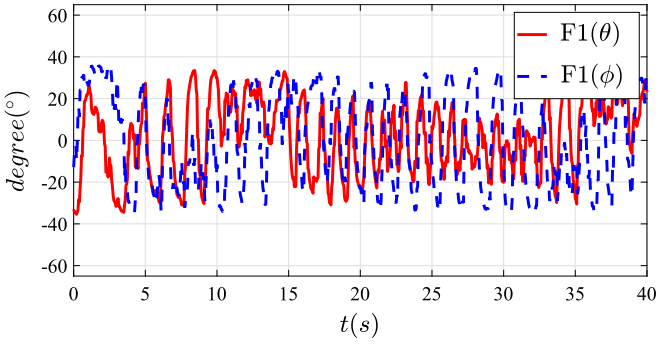

Fig. 24. Pitch θ and roll ϕ angles of follower 1 within 40 s in experiment 3.

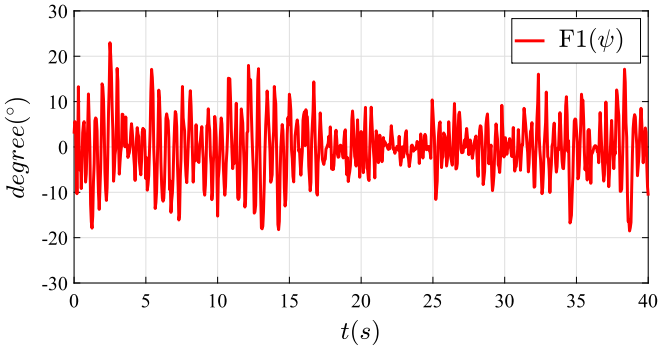

Fig. 25. Yaw ψ angle of follower 1 within 40 s in experiment 3.

7. Conclusions and future work

Continuous and discrete time-varying formation tracking problems for multi-UAV system were investigated, where the leader was subject to unknown dynamical control input. Using sliding mode control method, formation tracking controllers were constructed in continuous-time and discrete-time cases. Sufficient conditions for multi-UAV system to achieve the time-varying formation tracking were given, where the width of QSMD for discrete-time case was derived. Algorithms were summarized to show the procedure for designing the continuous and discrete time-varying formation tracking protocols. By utilizing seven quadrotor UAVs in Gazebo simulator, the virtual experiments demonstrated that the formation tracking can be realized with continuous and discrete protocols. The results of virtual formation tracking experiments showed that the designed protocols were effective and the error of formation tracking was reduced with the decrease of sampling time. In practical applications, the sampling time should be determined based on the minimum sampling time allowed by the digital system and the maximum acceptable formation error in order to make a tradeoff between efficiency and accuracy.

The formation tracking controller proposed in this paper was demonstrated by the Gazebo simulator. The future work is to perform the experiments with real UAVs to better verify the application of theoretical algorithms in engineering fields.

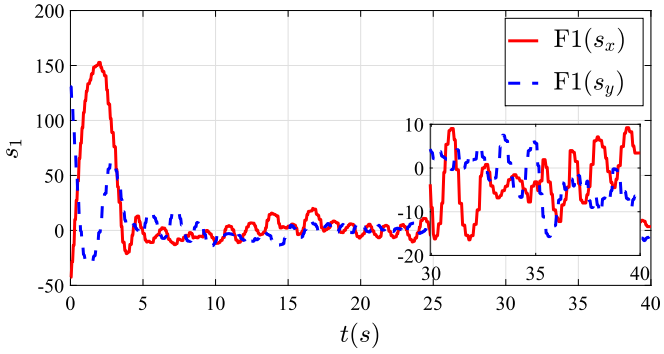

Fig. 26. Switching function $s_1(k)$ of follower 1 within 40 s in experiment 3.

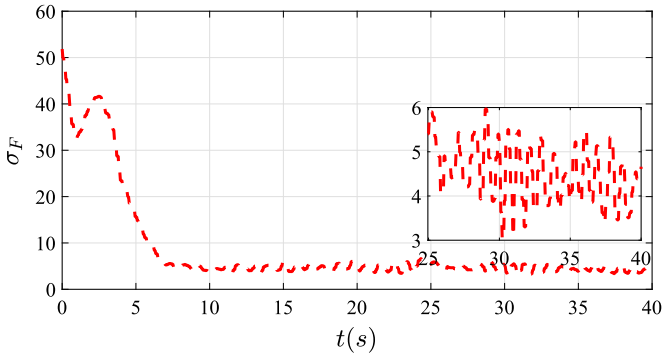

Fig. 27. Formation tracking error $\sigma_F(k)$ within 40 s in experiment 3.

Declaration of competing interest

The authors declare that they have no known competing financial interests or personal relationships that could have appeared to influence the work reported in this paper.

References

[1] B. Di, R. Zhou, H. Duan, Potential field based receding horizon motion planning for centrality-aware multiple UAV cooperative surveillance, Aerosp. Sci. Technol. 46 (2015) 386–397, https://doi.org/10.1016/j.ast.2015.08.006.
[2] C. Hu, Z. Zhang, N. Yang, H.-S. Shin, A. Tsourdos, Fuzzy multiobjective cooperative surveillance of multiple UAVs based on distributed predictive control for unknown ground moving target in urban environment, Aerosp. Sci. Technol. 84 (2019) 329–338, https://doi.org/10.1016/j.ast.2018.10.017.
[3] Y. Liu, H. Liu, Y. Tian, C. Sun, Reinforcement learning based two-level control framework of UAV swarm for cooperative persistent surveillance in an unknown urban area, Aerosp. Sci. Technol. 98 (2020) 105671, https://doi.org/10.1016/j.ast.2019.105671.
[4] Q. Hu, X. Shao, W. Chen, Robust fault-tolerant tracking control for spacecraft proximity operations using time-varying sliding mode, IEEE Trans. Aerosp. Electron. Syst. 54 (1) (2017) 2–17, https://doi.org/10.1109/TAES.2017.2729978.
[5] T. Chen, J. Shan, Continuous constrained attitude regulation of multiple spacecraft on so(3), Aerosp. Sci. Technol. 99 (2020) 105769, https://doi.org/10.1016/j.ast.2020.105769.
[6] Y. Zhai, X. Zhan, B. Pervan, Bounding integrity risk and false alert probability over exposure time intervals, IEEE Trans. Aerosp. Electron. Syst. 56 (3) (2019) 1873–1885, https://doi.org/10.1109/TAES.2019.2935962.
[7] Q. Hu, Y. Shi, C. Wang, Event-based formation coordinated control for multiple spacecraft under communication constraints, IEEE Trans. Syst. Man Cybern. Syst. (2019) 1–12, https://doi.org/10.1109/TSMC.2019.2919027.
[8] H. Lee, D. Yoo, B. Lee, G. Moon, D. Lee, M. Tahk, H. Shin, Parameter-robust linear quadratic Gaussian technique for multi-agent slung load transportation, Aerosp. Sci. Technol. 71 (2017) 119–127, https://doi.org/10.1016/j.ast.2017.09.014.
[9] M. Niu, X. Zhan, L. Liu, X. Su, A class of slce-based spreading codes for gnss use, IEEE Trans. Aerosp. Electron. Syst. 49 (1) (2013) 698–702, https://doi.org/10.1109/TAES.2013.6404137.
[10] S. Cao, Y. Li, J. Zhang, Y. Deguchi, Lagrangian analysis of mass transport and its influence on the lift enhancement in a flow over the airfoil with a synthetic jet, Aerosp. Sci. Technol. 86 (2019) 11–20, https://doi.org/10.1016/j.ast.2019.01.008.
[11] W. He, S. Zhang, Control design for nonlinear flexible wings of a robotic aircraft, IEEE Trans. Control Syst. Technol. 25 (1) (2016) 351–357, https://doi.org/10.1109/TCST.2016.2536708.
[12] W. He, Y. Ouyang, J. Hong, Vibration control of a flexible robotic manipulator in the presence of input deadzone, IEEE Trans. Ind. Inform. 13 (1) (2016) 48–59, https://doi.org/10.1109/TII.2016.2608739.
[13] S. Taamallah, X. Bombois, P.M. Van den Hof, Trajectory planning and trajectory tracking for a small-scale helicopter in autorotation, Control Eng. Pract. 58 (2017) 88–106, https://doi.org/10.1016/j.conengprac.2016.08.009.
[14] H. Li, X. Liao, T. Huang, W. Zhu, Y. Liu, Second-order global consensus in multiagent networks with random directional link failure, IEEE Trans. Neural Netw. Learn. Syst. 26 (3) (2014) 565–575, https://doi.org/10.1109/TNNLS.2014.2320274.
[15] Z. Li, J. Chen, Robust consensus of linear feedback protocols over uncertain network graphs, IEEE Trans. Autom. Control 62 (8) (2017) 4251–4258, https://doi.org/10.1109/TAC.2017.2685082.
[16] Y. Zheng, J. Ma, L. Wang, Consensus of hybrid multi-agent systems, IEEE Trans. Neural Netw. Learn. Syst. 29 (4) (2017) 1359–1365, https://doi.org/10.1109/TNNLS.2017.2651402.
[17] J. Xi, Z. Fan, H. Liu, T. Zheng, Guaranteed-cost consensus for multiagent networks with Lipschitz nonlinear dynamics and switching topologies, Int. J. Robust Nonlinear Control 28 (7) (2018) 2841–2852, https://doi.org/10.1002/rnc.4051.

[18] A. Abdessameud, A. Tayebi, Formation control of vtol unmanned aerial vehicles with communication delays, Automatica 47 (11) (2011) 2383–2394, https://doi.org/10.1016/j.automatica.2011.08.042.
[19] J. Seo, Y. Kim, S. Kim, A. Tsourdos, Consensus-based reconfigurable controller design for unmanned aerial vehicle formation flight, Proc. Inst. Mech. Eng., Part G, J. Aerosp. Eng. 226 (7) (2012) 817–829, https://doi.org/10.1177/0954410011415157.
[20] X. Dong, B. Yu, Z. Shi, Y. Zhong, Time-varying formation control for unmanned aerial vehicles: theories and applications, IEEE Trans. Control Syst. Technol. 23 (1) (2014) 340–348, https://doi.org/10.1109/TCST.2014.2314460.
[21] X. Dong, Y. Zhou, Z. Ren, Y. Zhong, Time-varying formation control for unmanned aerial vehicles with switching interaction topologies, Control Eng. Pract. 46 (2016) 26–36, https://doi.org/10.1016/j.conengprac.2015.10.001.
[22] L. He, P. Bai, X. Liang, J. Zhang, W. Wang, Feedback formation control of UAV swarm with multiple implicit leaders, Aerosp. Sci. Technol. 72 (2018) 327–334, https://doi.org/10.1016/j.ast.2017.11.020.
[23] Y. Xu, D. Luo, D. Li, Y. You, H. Duan, Target-enclosing affine formation control of two-layer networked spacecraft with collision avoidance, Chin. J. Aeronaut. 32 (12) (2019) 2679–2693, https://doi.org/10.1016/j.cja.2019.04.016.
[24] J.A. Guerrero, P. Castillo, Y. Challal, Trajectory tracking for a group of mini rotorcraft flying in formation, IFAC Proc. Vol. 44 (1) (2011) 6331–6336, https://doi.org/10.3182/20110828-6-IT-1002.03504.
[25] D. Mercado, R. Castro, R. Lozano, Quadrotors flight formation control using a leader-follower approach, in: 2013 European Control Conference (ECC), IEEE, 2013, pp. 3858–3863.
[26] A.T. Hafez, S.N. Givigi, S. Yousefi, Unmanned aerial vehicles formation using learning based model predictive control, Asian J. Control 20 (3) (2018) 1014–1026, https://doi.org/10.1002/asjc.1774.
[27] L. Han, X. Dong, Q. Li, Z. Ren, Formation tracking control for time-delayed multi-agent systems with second-order dynamics, Chin. J. Aeronaut. 30 (1) (2017) 348–357, https://doi.org/10.1016/j.cja.2016.10.019.
[28] J. Wang, M. Xin, Integrated optimal formation control of multiple unmanned aerial vehicles, IEEE Trans. Control Syst. Technol. 21 (5) (2012) 1731–1744, https://doi.org/10.1109/TCST.2012.2218815.
[29] X. Dong, Y. Li, C. Lu, G. Hu, Q. Li, Z. Ren, Time-varying formation tracking for UAV swarm systems with switching directed topologies, IEEE Trans. Neural Netw. Learn. Syst. 30 (12) (2018) 3674–3685, https://doi.org/10.1109/TNNLS.2018.2873063.
[30] Z. Zhen, G. Tao, Y. Xu, G. Song, Multivariable adaptive control based consensus flight control system for UAVs formation, Aerosp. Sci. Technol. 93 (2019) 105336, https://doi.org/10.1016/j.ast.2019.105336.
[31] J. Zhang, J. Yan, P. Zhang, Multi-UAV formation control based on a novel back-stepping approach, IEEE Trans. Veh. Technol. 69 (3) (2020) 2437–2448, https://doi.org/10.1109/TVT.2020.2964847.
[32] B. Zhang, X. Sun, S. Liu, X. Deng, Adaptive differential evolution-based receding horizon control design for multi-UAV formation reconfiguration, Int. J. Control. Autom. Syst. 17 (12) (2019) 3009–3020, https://doi.org/10.1007/s12555-018-0421-2.
[33] B. Yan, C. Wu, P. Shi, Formation consensus for discrete-time heterogeneous multi-agent systems with link failures and actuator/sensor faults, J. Franklin Inst. 356 (12) (2019) 6547–6570, https://doi.org/10.1016/j.jfranklin.2019.03.028.
[34] G. Xu, C. Huang, G. Zhai, A necessary and sufficient condition for designing formation of discrete-time multi-agent systems with delay, Neurocomputing 315 (2018) 48–58, https://doi.org/10.1016/j.neucom.2018.06.007.
[35] J. Hu, X. Sun, L. He, Time-varying formation tracking for multiple UAVs with nonholonomic constraints and input quantization via adaptive backstepping control, Int. J. Aeronaut. Space Sci. 20 (3) (2019) 710–721, https://doi.org/10.1007/s42405-019-00157-6.
[36] S. Li, J. Zhang, X. Li, F. Wang, X. Luo, X. Guan, Formation control of heterogeneous discrete-time nonlinear multi-agent systems with uncertainties, IEEE Trans. Ind. Electron. 64 (6) (2017) 4730–4740, https://doi.org/10.1109/TIE.2017.2674590.
[37] K. Guo, X. Li, L. Xie, Ultra-wideband and odometry-based cooperative relative localization with application to multi-UAV formation control, IEEE Trans. Cybern. 50 (6) (2019) 2590–2603, https://doi.org/10.1109/TCYB.2019.2905570.
[38] W. Song, J. Wang, S. Zhao, J. Shan, Event-triggered cooperative unscented Kalman filtering and its application in multi-UAV systems, Automatica 105 (2019) 264–273, https://doi.org/10.1016/j.automatica.2019.03.029.
[39] I. Bayezit, B. Fidan, Distributed cohesive motion control of flight vehicle formations, IEEE Trans. Ind. Electron. 60 (12) (2012) 5763–5772, https://doi.org/10.1109/TIE.2012.2235391.
[40] D. Mellinger, N. Michael, V. Kumar, Trajectory generation and control for precise aggressive maneuvers with quadrotors, Int. J. Robot. Res. 31 (5) (2012) 664–674, https://doi.org/10.1177/0278364911434236.
[41] S.P. Bhat, D.S. Bernstein, Finite-time stability of continuous autonomous systems, SIAM J. Control Optim. 38 (3) (2000) 751–766, https://doi.org/10.1137/S0363012997321358.
[42] W. Gao, Y. Wang, A. Homaifa, Discrete-time variable structure control systems, IEEE Trans. Ind. Electron. 42 (2) (1995) 117–122, https://doi.org/10.1109/41.370376.